JOURNAL OF QUATERNARY SCIENCE (2021) **36**(1) 20–28 ISSN 0267-8179. DOI: 10.1002/jqs.3245

JQS Journal of Quaternary Science QRA Quaternary Research Association

Testing the consistency of Holocene and Last Glacial Maximum spatial correlations in temperature proxy records

MARIA RESCHKE,[1,2]* IGOR KRÖNER[1,2] and THOMAS LAEPPLE[1,3]

[1]Alfred Wegener Institute Helmholtz Centre for Polar and Marine Research, Telegrafenberg A45, Potsdam, 14473, Germany
[2]Institute of Geosciences, University of Potsdam, Karl-Liebknecht-Straße 24/25, Potsdam, 14476, Germany
[3]MARUM – Center for Marine Environmental Sciences and Faculty of Geosciences, University of Bremen, Bremen, 28334, Germany

Received 7 October 2019; Revised 24 August 2020; Accepted 30 August 2020

ABSTRACT: Holocene temperature proxy records are commonly used in quantitative synthesis and model-data comparisons. However, comparing correlations between time series from records collected in proximity to one another with the expected correlations based on climate model simulations indicates either regional or noisy climate signals in Holocene temperature proxy records. In this study, we evaluate the consistency of spatial correlations present in Holocene proxy records with those found in data from the Last Glacial Maximum (LGM). Specifically, we predict correlations expected in LGM proxy records if the only difference to Holocene correlations would be due to more time uncertainty and more climate variability in the LGM. We compare this simple prediction to the actual correlation structure in the LGM proxy records. We found that time series data of ice-core stable isotope records and planktonic foraminifera Mg/Ca ratios were consistent between the Holocene and LGM periods, while time series of Uk'37 proxy records were not as we found no correlation between nearby LGM records. Our results support the finding of highly regional or noisy marine proxy records in the compilation analysed here and suggest the need for further studies on the role of climate proxies and the processes of climate signal recording and preservation.

KEYWORDS: Holocene; LGM; spatial correlation; temperature; Uk'37

Introduction

Palaeoclimate proxy records are invaluable for understanding past climate. Although limited in spatial coverage and affected by uncertainties (e.g. Breitenbach *et al.*, 2012; Lohmann *et al.*, 2013), proxy records are increasingly used in model-data comparisons (e.g. Lohmann *et al.*, 2013; Laepple and Huybers, 2014; Marsicek *et al.*, 2018) and quantitative syntheses (e.g. Gajewski, 2015; Harbert and Nixon, 2018; Luoto *et al.*, 2018). Thus, it is important to understand the climate signal recorded by proxies and the related uncertainties.

One way to characterize the proxy signal is to compare how records from the same site replicate (e.g. Fisher *et al.*, 1985; DeLong *et al.*, 2007) or to examine similarities between records collected in close spatial proximity to one another (e.g. Münch *et al.*, 2016, 2017). These studies are often limited to the last millennium (e.g. Stephans *et al.*, 2004; DeLong *et al.*, 2013) and the Holocene (e.g. Reschke *et al.*, 2019a).

Reschke *et al.* (2019a) empirically estimated signal-to-noise ratios in compilations of temperature proxy data from the Holocene by comparing the correlations in time series from sites that are in close spatial proximity to one another to those obtained from climate model-derived time series from the same proxy sites and time period. They found an unexpectedly low correlation among neighbouring proxy sites in contrast to a strong correlation predicted by climate models, indicating either noisy proxy records or climate variations that vary on spatial scales that are too small to be captured by the relatively large-scale climate models.

*Correspondence: M. Reschke, as above.
E-mail: mreschke@awi.de

As the Holocene is a climate state that is relatively stable, we extend previous investigations of the spatial correlation structure of proxy records (Reschke *et al.*, 2019a), i.e. the similarity of proxy time series depending on the separation distance of sites, to a different climate state with a higher variability in the temperature proxy data: the Last Glacial Maximum (LGM). This provides a further test of the current understanding of the proxy signals. Specifically, we analyse for the first time the correlation structures between temperature proxy records in the LGM and test whether they are consistent with the spatial correlations found in Holocene temperature proxy records. First, we investigate the processes that may cause differences between the correlation structures of the Holocene and LGM such as the amount of climate variability relative to the noise component and the amount of time uncertainty. Then, we predict spatial correlations of surrogate time series for the LGM generated based on spatial correlations of Holocene temperature proxy data by accounting for these known processes and compare these expected LGM spatial correlations with estimates of the spatial correlation structure based on LGM temperature proxy records.

Data

The focus of this study is the comparison of the spatial correlation structure (i.e. the correlation of time series in dependence of the separation distance of proxy sites) of proxy records of two different climate states, i.e. the Holocene and the LGM, with a similar amount and quality of available high-resolution temperature proxy records. Thus, we analyse the existing high-resolution globally distributed multi-archive and

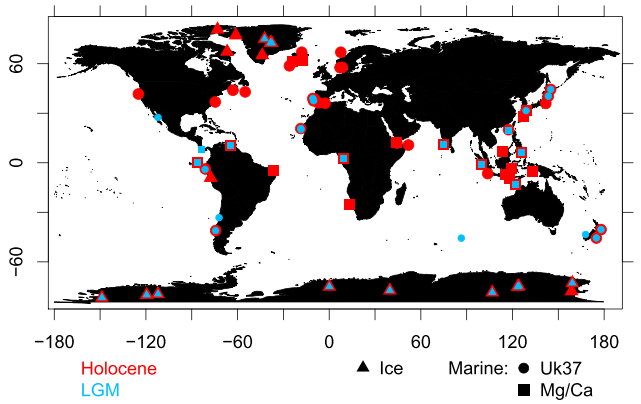

Figure 1. Overview of the Holocene and LGM proxy dataset. Site locations show the selection of time series from the compilation of Rehfeld *et al.* (2018) which are analysed in this study. Proxy types are indicated by symbols. For Holocene and LGM data at the same site the symbols of the time periods overlie each other. [Color figure can be viewed at wileyonlinelibrary.com]

multi-proxy dataset of Holocene and LGM temperature proxy records of Rehfeld *et al.* (2018). Originally compiled to compare Glacial and Holocene temperature variability, this collection compiled available published records that have an established calibration to temperature, cover at least a 4-ka interval during an 8-ka period during the LGM (27–19 ka BP) and/or the Holocene (8–0 ka BP), and are available at a mean sampling frequency of at least 1/225 a^{-1} (Rehfeld *et al.*, 2018). To have consistent Holocene and LGM datasets, we only used the three most common proxy types available for both time periods: (i) ice-core stable isotope records, (ii) marine sediment time series reconstructed from Uk'37 and (iii) planktonic foraminifera Mg/Ca ratios. This yielded 64 time series for the Holocene and 36 for the LGM (Fig. 1; Table 1; Supporting Information Table S1). For the marine records, we use the temperature calibrations of the original studies, while for the ice-core-based time series we use the recalibration of Rehfeld *et al.* (2018). As our study is based only on correlations, the results are largely independent of the calibration choice.

Methods

Approach and assumptions

We estimate the correlation of paired temperature-related proxy time series as a function of distance (spatial correlation) for the Holocene records ($\rho_{\mathrm{Hol,Prx}}$) and the LGM proxy records ($\rho_{\mathrm{LGM,Prx}}$). To test the current understanding of proxy signals by testing the consistency of the spatial correlation structure of temperature proxy records for different climate states, we then predict the spatial correlation expected for LGM proxy records based on the Holocene spatial correlations assuming that the correlation differences are caused only by a different amount of climate variability and time uncertainty between both climate states. Then, we compare these predicted correlations based on LGM surrogate time series ($\rho_{\mathrm{LGM,tu}}$) with the observed correlations in LGM proxy records (Fig. 2).

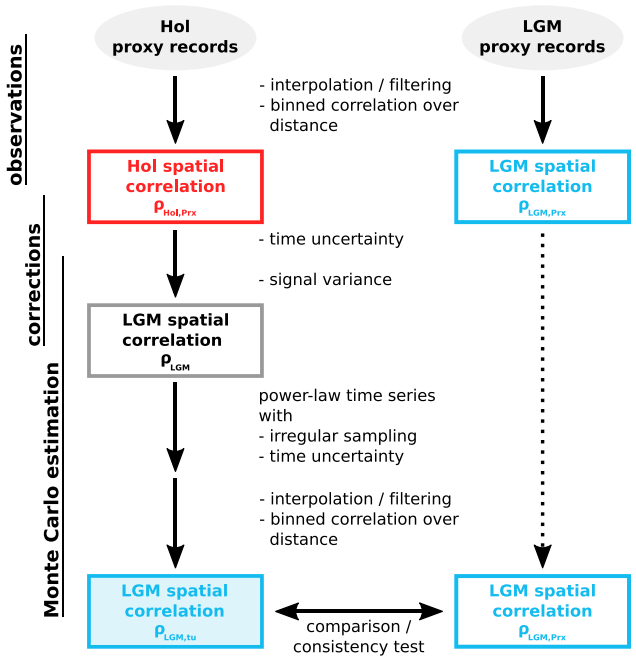

Figure 2. Processing steps for the Holocene and LGM data. Proxy records are used to estimate the Holocene and LGM spatial correlations. Corrections are applied to the Holocene spatial correlations to estimate the expected spatial correlations of LGM surrogate time series in a Monte Carlo procedure. A comparison of the proxy- and surrogate-based spatial correlations for the LGM is used to test the consistency of Holocene and LGM spatial correlations of proxy records. [Color figure can be viewed at wileyonlinelibrary.com]

Consistency between the observed and predicted correlations would indicate that we captured the main processes affecting the correlation structure and provide support for the low Holocene correlation estimates of Reschke *et al.* (2019a) although the level of consistency, and thus the degree of confirmation, hinges on the estimation uncertainty. If the results should turn out to be very different, this would challenge our current approaches to interpreting proxy records.

To predict the LGM spatial correlations, we assume that temperature proxy records consist of a climate signal and a noise component related to non-climate-related factors (e.g. different sampling protocols or a varying sedimentation rate). Furthermore, we make the following two assumptions and discuss their implications later: (i) the LGM climate system has the same or greater spatial correlations as the Holocene (based on our analyses of climate model simulations for both time periods), i.e. that paired temperature proxy records are more similar in the LGM than in the Holocene, e.g. due to a stronger variability in the LGM temperature signal; and (ii) the noise component related to non-climate-related factors is independent of the climate state: most error sources such as measurement uncertainties and aliasing due to a finite number of samples are – to a first approximation – independent of the mean climate state and should therefore be similar in either time period (Laepple and Huybers, 2013; Dolman and Laepple, 2018; Laepple *et al.*, 2018).

Compared to the Holocene we then expect differences in the proxy correlations due to a generally higher climate

Table 1. Overview of the Holocene and LGM dataset of Rehfeld *et al.* (2018). Only the proxy types in bold type are used in this study.

	Sum of records	Uk'37	Mg/Ca	**TEX_{86}**	Terrestrial bio-indicator	Ice-core stable isotopes	Other
Holocene	88	**27**	**19**	4	11	**18**	9
LGM	39	**15**	**9**	2	–	**12**	1

variability (Rehfeld *et al.*, 2018) and larger time uncertainty in the LGM. Changes in climate variability are estimated from the variance ratios $\sigma^2_{LGM}/\sigma^2_{Hol}$ of LGM and Holocene proxy records (Rehfeld *et al.*, 2018), while typical time uncertainties of LGM and Holocene proxy data are estimated using the datasets of Shakun *et al.* (2012) and Marcott *et al.* (2013).

Holocene and LGM spatial correlation structure from climate model simulation

To gain an indication about possible differences in the spatial correlation structure between Holocene and LGM temperature proxy records we first rely on climate model simulations. We analysed the spatial correlation structure of (unfiltered) annual means of surface air temperatures extracted from ECHAM5/MPI-OM equilibrium model simulations of the Mid-Holocene (788 years; Wei and Lohmann, 2012) and the LGM (1000 years; Zhang *et al.*, 2013). Data were extracted at grid cell level to estimate the correlations R as a function of site separation x. Then, the correlation decay length l_d (i.e. the site separation at which the correlation of paired time series decayed to $1/e$ of the correlations of replicate cores) of the Mid-Holocene and LGM is estimated by fitting an exponential, $R = e^{-x/l_d}$, to the decay of correlations. The overall magnitude and structure of the correlation decay length is similar in both climate states (Fig. 3). During the LGM (2910 km), the mean interannual correlation decay length, l_d, is higher compared to the Holocene (2080 km) with the strongest differences in the tropics and in the northern hemisphere. This Holocene result is consistent with findings (2240 km) by Reschke *et al.* (2019a) who used data from a 6-ka Holocene model simulation by Fischer and Jungclaus (2011).

We note that due to the unavailability of long LGM simulations, this analysis was performed on annual data, whereas the remaining study is based on centennial to millennial variations that are also affected by forcing factors (e.g. transient changes in insolation) not considered in the analysed simulations. Thus, we expect a higher spatial correlation with higher correlation decay lengths (5000 km) when considering climate variability on centennial to millennial time scales (Laepple and Huybers, 2014; Reschke *et al.*, 2019a). Still, the similarity between the Holocene and LGM decay lengths of interannual data suggests that the general spatial correlation structures are a first-order property of the climate system that is only weakly affected by the mean climate state.

Effect of changes in climate variability on the predicted correlations

Different palaeoclimate archives suggest a higher climate variability during the LGM (e.g. Ditlevsen *et al.*, 1996; Rehfeld *et al.*, 2018). Assuming the simplest possible model, we assume that our temperature proxy-based time series consist of two components – a climate signal S and an independent random (white) noise ε. Thus, two proxy time series X and Y can be described as $X = S + \varepsilon_x$ and $Y = S + \varepsilon_y$ where the signal and noise components of both time series are uncorrelated, i.e. $cor(S,\varepsilon_x) = cor(S,\varepsilon_y) = cor(\varepsilon_x,\varepsilon_y) = 0$. We can then derive the expected correlation in the LGM, ρ_{LGM}, from the correlation in the Holocene, ρ_{Hol}, using

$$\rho_{LGM}(z) = \frac{z}{(z-1) + \rho_{Hol}^{-1}} \quad (1)$$

where z is the assumed variance change between the Holocene and LGM climate signals ($\sigma^2_{LGM}/\sigma^2_{Hol}$) (Appendix A). For a constant variance of the noise component, but a different variance of the signal component for the Holocene and LGM, changes in the variance ratio of the climate signal z of proxy records could indicate a reduction (for $z < 1$) or an increase (for $z > 1$) in the initial correlation, cor_0, with the strongest changes occurring for $cor_0 \approx 0.5$ (Fig. 4A).

Effect of changes in time uncertainty on the predicted correlations

We generally expect time uncertainty to increase as we go further back in time, i.e. the time uncertainty of age models based on radiocarbon dating should be higher for the LGM than for the Holocene records, e.g. due to reservoir effects (Ascough *et al.*, 2005). The effect of time uncertainty on the correlation of time series depends on four factors: (i) the magnitude and temporal structure of time uncertainty, with higher time uncertainties leading to a stronger reduction in correlation; (ii) the initial correlation cor_0 of annually resolved time series without time uncertainty; (iii) the temporal structure

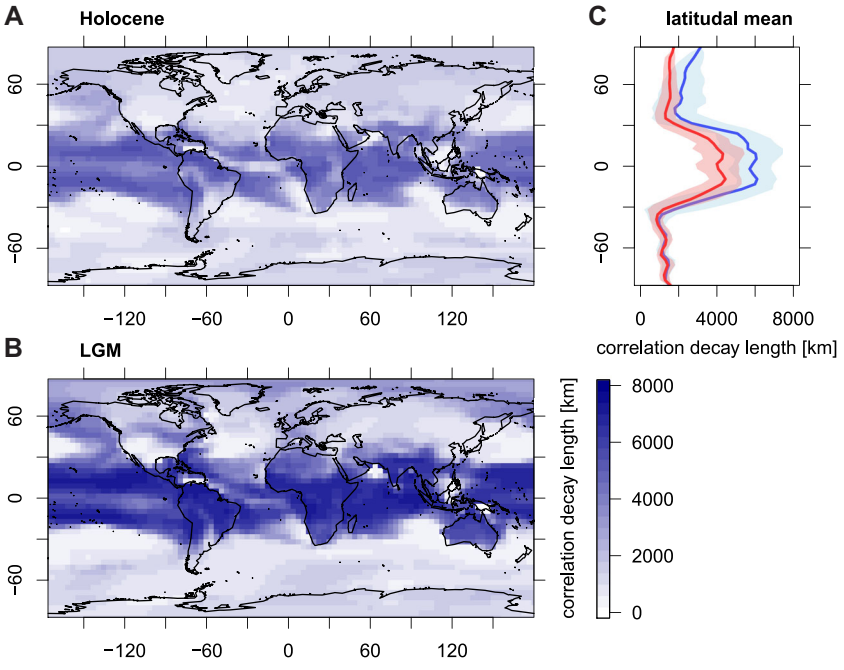

Figure 3. Spatial correlation decay length during (A) the Mid-Holocene and (B) LGM, and (C) latitudinal mean of the correlation decay length. The estimates are based on Mid-Holocene (Wei and Lohmann, 2012) and LGM (Zhang *et al.*, 2013) air surface temperatures from an equilibrium model simulation of the ECHAM5/MPI-OM. The LGM is characterized by higher correlation decay lengths in the tropics and in the Northern Hemisphere than the Holocene. Shaded areas depict the area of $\pm\sigma$ (standard deviation) of the correlation decay length estimates for the latitudes. [Color figure can be viewed at wileyonlinelibrary.com]

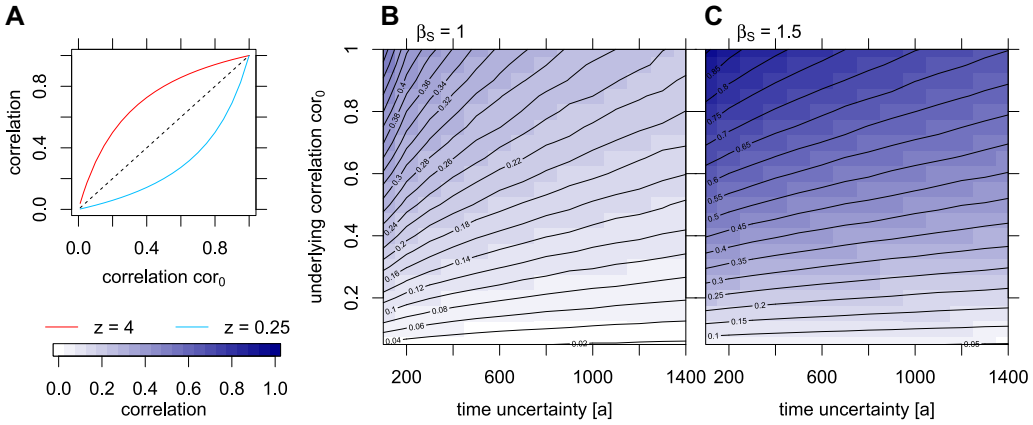

Figure 4. Effects of signal variance (A) and time uncertainty on the correlation of time series for a climate signal with weaker (B) and stronger (C) climate variability. Changes in the variance of the climate signal by a factor of z cause a reduction (for $z < 1$) or a rise (for $z > 1$) of the correlation cor_0 in correlation estimates. For red noise climate signals time uncertainty decreases the correlation cor_0. The higher the time uncertainty, the stronger is the decrease of cor_0. [Color figure can be viewed at wileyonlinelibrary.com]

(power spectrum) of the climate signal (rapidly varying signals are more susceptible to time uncertainty); and (iv) the timescale on which the correlation is estimated if the noise and the climate signal components have different temporal structures (Reschke *et al.*, 2019b).

For simplicity, we assumed that the climate variability in point (iii) can be approximated as having a power-law scaling with a power spectral density $PSD = f^{-\beta_S}$, where f is the frequency and β_S the slope of the climate signal. Such a scaling has been found to be a good description of Quaternary climate variability (e.g. Huybers and Curry, 2006; Laepple and Huybers, 2014).

As we are not aware of analytical expressions quantifying the effect of time uncertainty on the correlation structure, we rely on numerical simulations. To simulate time uncertainty, we defined control points at certain ages and shifted them by adding a random value from a normal distribution (with zero mean and a standard deviation equal to the time uncertainty). A new time axis is then created by linearly interpolating between the control points.

To illustrate the effect of time uncertainty on the correlation of time series, we apply different time uncertainties to 50-ka surrogate time series. As the applied procedure is also used for further analyses (described in next subsection) it is explained here in detail.

We performed a Monte Carlo procedure with 5000 repetitions. This yielded two 50-ka surrogate time series that each consisted of the superposition of an annual red noise (Huybers and Curry, 2006) power-law climate signal with a shallow ($\beta_S = 1$; Laepple and Huybers, 2014) or steeper slope ($\beta_S = 1.5$; if we also take the deglaciation into account) as well as annual non-climate-related factors which were collectively included as an independent (white) noise component ($\beta_N = 0$). The initial correlation of paired surrogate time series, cor_0, was in the range 0.05–1. The time uncertainties of the surrogates were applied to control points every 10 ka and ranged from 100 to 1400 years. These values are similar to the age uncertainties obtained by Shakun *et al.* (2012) (127 to 1304 years) for the time window of 27–19 ka BP. As the application of time uncertainty generates an irregular sampling of the surrogate time series, we use the method described by Reschke *et al.* (2019b), which applies a linear interpolation of the irregular time series onto a regular grid ($\Delta t = 10$ years) subjected to a Gaussian filter with cut-off frequency f_c, to determine the timescale-dependent correlations over a range of 2 to 1000 years, i.e. cut-off frequencies f_c from 1/2 to 1/1000 a^{-1}.

The correlation of time series thus decreases with increasing time uncertainty and this effect is even more pronounced for higher initial correlations cor_0 (Fig. 4B,C). Furthermore, weaker trends in climate signals lead to a stronger decrease in cor_0 (Fig. 4B vs Fig. 4C). Additionally, for climate signals with red noise spectra, correlations related to longer timescales (i.e. lower cut-off frequencies) are higher than for shorter ones (Supporting Information Fig. S1) which counteracts the decrease in correlation due to time uncertainty.

Estimating the surrogate-based LGM spatial correlation and accounting for parameter uncertainty

Based on Holocene proxy records we use a four-step approach to predict the expected LGM spatial correlation $\rho_{LGM,tu}$ of surrogate time series (cf. Fig. 2). (i) We estimated the Holocene correlation structure of (time-uncertain) proxy data, $\rho_{Hol,Prx}$. (ii) We corrected for the effect of time uncertainty to derive the underlying Holocene correlations of time-certain proxy data, ρ_{Hol}. For this step, we rely on an empirical transfer function (for a time uncertainty of 220 years) mapping the time-certain and time-uncertain correlations based on surrogate data (similar to the subsection above). (iii) We accounted for the expected differences in climate variability of Holocene and LGM proxy records to estimate the LGM correlation structure without time uncertainty, ρ_{LGM} (see 'Effect of changes in climate variability on the predicted correlations' above). (iv) We accounted for the time uncertainty and the uncertainty of a finite set of irregularly sampled finite time series by estimating the correlation $\rho_{LGM,tu}$ and its uncertainty on irregular time-uncertain surrogate time series.

In detail, we estimated the Pearson correlation between Holocene time series pairs for climate variability on millennial time scales (1000 years) using linear interpolation and Gaussian filtering (see Reschke *et al.*, 2019a). Holocene spatial correlations, $\rho_{Hol,Prx}$, were estimated using 2000-km bin sizes. As very distant sites will be essentially uncorrelated, we only considered spatial separations of up to 6000 km as previous studies suggest a correlation decay length of 5000 km for climate variability on centennial to millennial timescales (Laepple and Huybers, 2014; Reschke *et al.*, 2019a). Then, we corrected the time uncertainty (a Holocene-typical value of 220 years; based on the dataset of Marcott *et al.*, 2013) to derive the time-certain spatial correlation ρ_{Hol}.

We use a Monte Carlo approach (5000 repetitions) similar to the one described in the subsection above to predict LGM spatial correlations:

1. We estimated the expected spatial LGM correlation ρ_{LGM} (without time uncertainty) for irregularly sampled time series (Equation 1) while accounting for the uncertainty of the variability change by taking z from a normal distribution (mean $\mu = 4.4$, standard deviation $\sigma = 1.15$; Rehfeld *et al.*, 2018).
2. We accounted for the finite number of LGM time series of the proxy compilation by generating n (= the number of time series pairs per 2000-km-wide bin) power-law surrogate time series pairs ($\beta_S = 1$ or $\beta_S = 1.5$, $\beta_N = 0$, 8-ka length, annual resolution) with a correlation ρ_{LGM0} (= ρ_{LGM} for annually sampled unfiltered time series). Accounting for the finite samples per time series and the irregular sampling, we subsampled the time series according to a sampling typical for proxy records. The observations t_i were generated using block averaging of all observations between half the difference to the previous observation time ($t_i - \Delta t_i/2$) and half the difference to the next observation time ($t_i + \Delta t_{i+1}/2$) (cf. Reschke *et al.*, 2019b).
3. A plausible range of time uncertainty is taken into account by adding random values from a normal distribution (with zero mean whose standard deviation corresponds to the time uncertainty) to the control points of the surrogate time series (1 year, 4 ka, 8 ka). The time uncertainties were chosen from a normal distribution using different LGM-typical values based on the dataset of Shakun *et al.* (2012) for each surrogate time series (marine sediments: $\mu = 460$ years, $\sigma = 191$ years; ice-cores: $\mu = 290$ years, $\sigma = 120$ years).
4. Individual correlations of the surrogate time series pairs are then estimated at millennial timescales following the method (linear interpolation and Gaussian filtering) presented by Reschke *et al.* (2019b). We estimated the binned (2000 km) LGM mean correlation ($\rho_{LGM,tu}$) for separation distances up to 6000 km and the corresponding confidence interval (90% quantile) based on the number of repetitions of the Monte Carlo approach.

To test the consistency of the Holocene and LGM spatial correlations of proxy records we compared the expected results of spatial correlations from the surrogate LGM time series ($\rho_{LGM,tu}$) to those estimated from LGM proxy records ($\rho_{LGM,Prx}$). Following Reschke *et al.* (2019a), to determine the significance of proxy-based Holocene and LGM spatial correlations, we estimated confidence intervals of the null hypothesis of uncorrelated proxy data (90% quantiles) based on uncorrelated surrogate time series. This approach considers the total number of correlation pairs according to each bin.

Results

We estimated proxy-based Holocene spatial correlations, $\rho_{Hol,Prx}$, for all combinations of Uk'37, Mg/Ca and ice-core stable isotopes time series independent of the proxy types as we assume that the difference between sea surface and air surface temperatures are negligible due to an indicated coupling of near surface air and sea surface temperatures (Morice *et al.*, 2012). The correlation estimates are fairly constant at 0.2 for spatial separations up to 6000 km and statistically significant (Fig. 5A). This is slightly higher than the value of 0.18 found by Reschke *et al.* (2019a) and is probably the consequence of the use of a subset of their dataset and a time window of 8 ka instead of 6 ka in the present study. Correcting for the expected bias due to time uncertainty (assuming a climate signal with a spectral slope of $\beta_S = 1$) slightly increased the correlations to a mean value of 0.23 (ρ_{Hol}). Accounting for a stronger expected climate variability in the LGM, ρ_{LGM} resulted in an increase to 0.55, although this increase has a considerable uncertainty associated with it due to the uncertain increase in climate variability. Applying an LGM-typical time uncertainty reduced the predicted spatial correlation to $\rho_{LGM,tu} \approx 0.4$. In contrast to this expectation, the estimated proxy-based LGM spatial correlation, $\rho_{LGM,Prx}$, is zero except for the spatial separations below 2000 km where it is 0.26.

As there are proxy-specific recordings of the climate component, e.g. a habitat-dependent seasonal and depth-specific recording of organism-based proxies (Leduc *et al.*, 2010; Lohmann *et al.*, 2013), we examined the effect that different organism-based proxy types (i.e. alkenone Uk'37, planktonic foraminifera Mg/Ca) can have on the results. Thus, we consider pairs of Uk'37, Mg/Ca and ice-core stable isotopes time series combining only the same proxy types (Fig. 5B). The estimated spatial correlations are generally slightly higher, although not too different from the mixed results (Fig. 5A) and still indicate an inconsistency between the predicted and observed LGM spatial correlations.

To further elucidate possible proxy type-specific effects, we separately analysed the Uk'37 proxy, which yielded higher Holocene correlations (0.47) than the combined proxy types (Fig. 5C). Correcting for the time uncertainty led to slight increases in ρ_{Hol} (to 0.53), while accounting for the expected higher LGM climate variability led to an even stronger increase (to $\rho_{LGM} \approx 0.81$). Adding time uncertainty reduces the correlation ($\rho_{LGM,tu} \approx 0.52$). In contrast, the estimated LGM correlation of the Uk'37 proxy data $\rho_{LGM,Prx}$ is either close to zero or negative and thus indicates an even stronger inconsistency between the predicted and observed LGM correlations.

As the number of records is too low for Mg/Ca and ice-core stable isotopes to be analysed separately, we chose to analyse both proxy types together in all combinations of time series independent of the proxy type (Fig. 5D) to raise the statistical robustness of the correlation estimates. $\rho_{Hol,Prx}$ was 0.18 for separations below 2000 km and close to zero for greater separations. These values increased only slightly after removing time uncertainty (ρ_{Hol}). Accounting for a higher LGM climate variability increases the correlations yielding $\rho_{LGM} \approx 0.52$ for separations below 2000 km and 0.21 otherwise. Adding time uncertainty decreased $\rho_{LGM,tu}$ to 0.4 for separations below 2000 km and to 0.17 otherwise. For the combination of these two proxy types, the observed range of proxy-based LGM spatial correlations ($0.05 < \rho_{LGM,Prx} < 0.4$) falls within the uncertainty range of $\rho_{LGM,tu}$, thus indicating consistency between the predicted and observed LGM correlations.

We tested the effect of the use of different proxy types for paired time series on the results by using pairs of Mg/Ca and ice-core stable isotope time series combining only the same proxy types (Fig. 5E). As above, the spatial correlations are generally slightly higher for analysis of the same proxy types but remain similar to the mixed results (Fig. 5D). This also lends support to our previous finding that LGM spatial correlations and our predictions are consistent for these proxy types. These results are particularly sensitive to our assumption of the climate signal because a spectral slope of $\beta_S \approx 1.5$ leads to similar results (Supporting Information Fig. S2).

Discussion

We estimated the correlation of Holocene and LGM proxy time series for different spatial separations of the sites and used the Holocene spatial correlations to predict the expected LGM spatial correlations using surrogate power-law time series. Both the proxy-based and the predicted spatial LGM correlations were largely consistent for time series reconstructed from

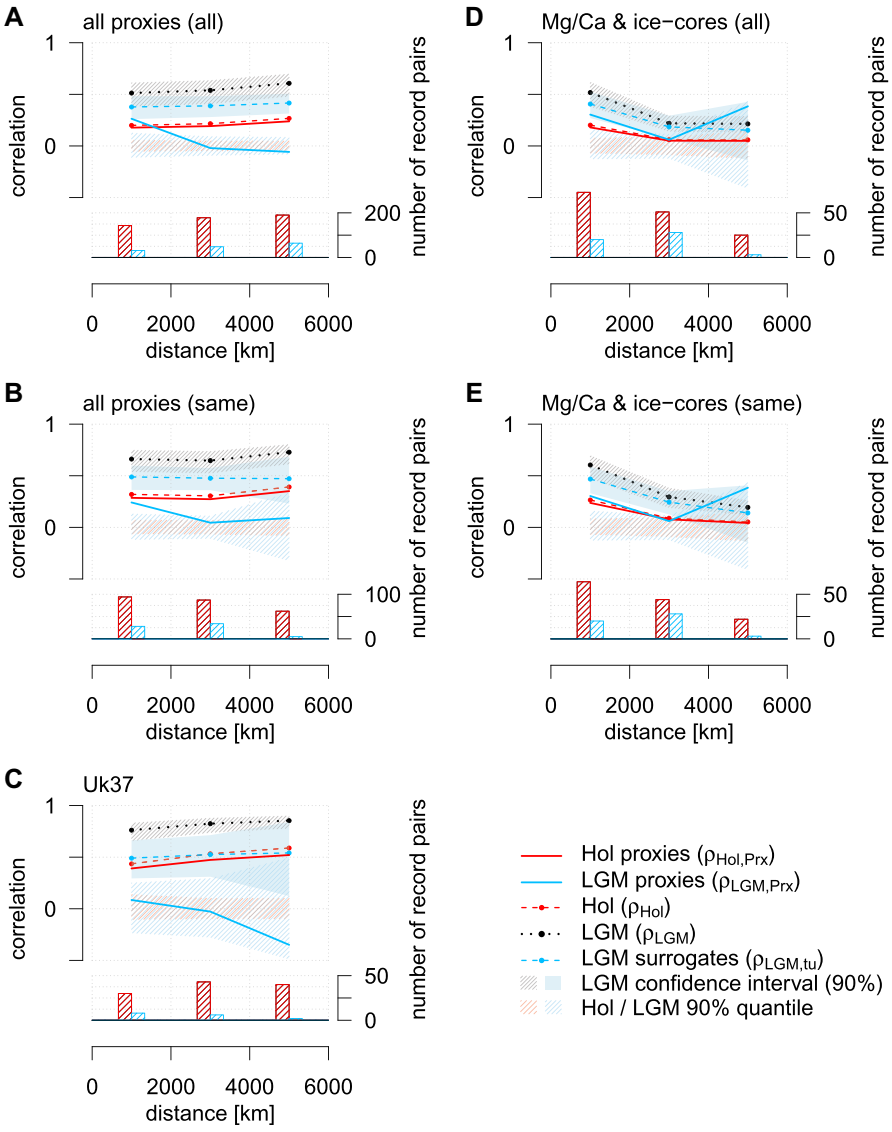

Figure 5. Spatial correlation (upper panel) and number of proxy record pairs (lower panel) for the Holocene and LGM. Correlations over distance are summarized in 2000-km-wide bins. The expected spatial correlation for the LGM is based on the reconstructed Holocene spatial correlations without time uncertainty and assumes a higher variance of the signal component ($\mu = 4.4$, $\sigma = 1.15$). The expected correlation of time-uncertain LGM records and its confidence interval (i.e. 90% quantiles) is based on a Monte Carlo procedure with 5000 repetitions applying a time uncertainty of 450 years on time series with a spectral slope of the climate signal of $\beta_S = 1$. 90% quantiles of the spatial correlations of uncorrelated Holocene and LGM surrogate data are used as a significance test for the proxy-based spatial correlations. Note that in D and E the correlation estimates between 4000 and 6000 km are based only on Mg/Ca and/or Mg/Ca vs. ice-cores as no ice-core pair at this distance is available. [Color figure can be viewed at wileyonlinelibrary.com]

planktonic foraminifera Mg/Ca and ice-core stable isotopes. In contrast, data compilations containing time series based on Uk'37 resulted in inconsistent proxy-based and predicted correlations as the spatial correlations in LGM Uk'37 datasets were surprisingly low. In the following, we discuss possible reasons for the different behaviour of the proxy types.

Proxy-specific recording and finite number of records

In our study, we assumed that all proxy types were recording the same climate component. However, the processes of climate recording and preservation are known to be proxy-specific, which limits the validity of our assumption. For example, marine organism-based proxies show a habitat-dependent seasonal and depth-specific recording (Leduc *et al.*, 2010; Lohmann *et al.*, 2013) and preferred dissolution of shells (Lea, 2003). While parts of this proxy-specific recording are accounted for in the proxy-specific temperature calibrations, other parts will persist and lead to systematic errors. This could lead to a potential underestimation of the Holocene and LGM spatial correlations depending on the chosen proxy type. Thus, our finding that spatial correlations using different proxy types (Fig. 5A,D) showed slightly lower (difference not statistically significant) correlations than the same correlations using the same proxy types (Fig. 5B,E) is consistent with the expectation that correlations of mixed-proxy-type analyses are less similar than those of single-proxy-type analyses due to the comparison of, for example, summer atmospheric temperature vs. mixed-layer winter temperature. This suggests that one should use proxy-specific and expert-driven knowledge for analyses and interpretations of individual sites.

Nevertheless, these effects should act in both climate states and thus do not explain the inconsistency we observed between the strong Holocene correlations and missing LGM spatial correlations (Fig. 5C) in the Uk'37 proxy records.

Time uncertainty of proxy records

While our analysis accounted for uncertainties in radiocarbon dating of sediment cores, this did not include uncertainties resulting from assumptions about reservoir age or the spatial and temporal variation of reservoir ages (Ascough *et al.*, 2005) which depend on the (local) climate and oceanic circulation patterns. In particular, polar waters and sea ice can exhibit higher reservoir ages. Studies of the Younger Dryas and Early Holocene reservoir ages have shown an increase by 300–400 years in glacial conditions (Haflidason *et al.*, 2000) compared to the current reservoir ages of 200–400 years for the mixed layer of the oceans (Stuiver *et al.*, 1986). The true time uncertainty, especially for the LGM, might therefore be higher due to these time-variable reservoir effects. Our estimates of the Holocene spatial correlation ρ_{Hol} (without time uncertainty) might therefore be too low, causing an underestimation

of the predicted LGM correlations ρ_{LGM} (without time uncertainty) and possibly an overestimation of the expected LGM correlations $\rho_{LGM,tu}$ (with time uncertainty). However, even a doubling of the assumed time uncertainty for the LGM (to 900 years) while keeping the time uncertainty of the Holocene would not be capable of reducing $\rho_{LGM,tu}$ to the low values we obtained for the current proxy-based LGM estimate $\rho_{LGM,Prx}$ (see also Supporting Information Fig. S2 $f_c = 1/1000$ years).

Contrary behaviour of Uk'37 records

For Uk'37 LGM proxy records, the correlation of the proxy time series ($\rho_{LGM,Prx}$) was indistinguishable from zero and fell outside the range of the predicted $\rho_{LGM,tu}$ values (Fig. 5C). This either indicates that the Uk'37 proxy recorded a climate signal that is spatially more coherent in the Holocene or that the Uk'37 time series are more corrupted by non-climate effects in the LGM compared to the Holocene. It is conceivable that the stronger climate variations in the LGM are also accompanied by more complex signals such as changes in water masses (and thus nutrients) or a stronger seasonality that would increase the level of non-temperature effects on the LGM records. One other possibility is that the high correlations in the Holocene records may be the result of spatially coherent non-climatic effects in the Holocene Uk'37 proxy signal.

The results for the Uk'37 record stand out, as those for other proxy types (planktonic foraminiferal Mg/Ca, ice-core stable isotopes) were consistent in both $\rho_{LGM,Prx}$ and $\rho_{LGM,tu}$. A different behaviour in Uk'37- and Mg/Ca-based temperature reconstructions has already been described in previous studies (e.g. Lohmann *et al.*, 2013; Liu *et al.*, 2014; Marsicek *et al.*, 2018) where these discrepancies are attributed to different ecological (e.g. habitat depth) and seasonal (e.g. production season) biases of the proxy carrier, whereas others attributed these discrepancies to regional differences in the distribution of different proxy records (e.g. Mix *et al.*, 2000; Mix, 2006; Leduc *et al.*, 2010), or to re-deposition and post-depositional effects (e.g. Hoefs *et al.*, 1998; Gong and Hollander, 1999; Ohkouchi *et al.*, 2002; Regenberg *et al.*, 2006).

Furthermore, the number and distribution of Uk'37 time series differ between the Holocene and LGM, with a particular scarcity of LGM time series in the North Atlantic (Fig. 1). The strong linear cooling trend present in most Holocene Uk'37 time series favours an overestimation of the spatial correlation at distances between 2000 and 6000 km. Due to the lack of LGM data from the North Atlantic, we cannot currently test the hypothesis of higher spatial correlations due to stronger trends recorded by Uk'37 in Holocene time series. As this study requires the use of high-resolution time series, which are common in the coastal and continental shelf regions, the analysis of sets of time series for the area of the deeper ocean (e.g. the central North Atlantic) covering the Holocene and LGM is not possible as there is generally a lower resolution of the proxy records due to lower sedimentation rates of the deeper ocean.

Spatial correlation structure and orbital trends

Model simulations suggested a higher spatial correlation during the LGM (Fig. 3) which seems to contradict our proxy-based results (Fig. 5). While our model-based estimates of the correlation structure are based on an equilibrium model simulation that is not orbitally forced, the proxy records contain orbitally forced temperature trends and seasonal temperatures which can create large-scale patterns and thus affect the correlation structure (e.g. Lohmann *et al.*, 2013). It has been suggested that such patterns and also differences between proxy types could be explained by seasonal recordings of orbitally driven trends in the Holocene (Leduc *et al.*, 2010). However, by evaluating insolation and seasonal temperature trends in the Holocene and LGM, we did not find any systematic differences in the amplitude of the orbital trends between either time period (Supporting Information Fig. S3).

Expanding the time window of proxy time series

It is possible to increase the number of proxy records and thus the robustness of the analyses presented in this study by extending the time window covered by the time series, e.g. by considering Marine Isotope Stage (MIS) 2 (29–14 ka BP) instead of the LGM (27–19 ka BP) or analysing MIS 1 (14–0 ka BP) instead of the Holocene (8–0 ka BP). On the one hand, a longer time window is required to analyse spatial correlations related to, for example, climate variability on timescales >2 ka and thus to allow the use of a higher number of low-resolution time series from the central oceans.

Furthermore, we expect higher correlations for MIS 2 compared to the LGM as there should be stronger temperature signals due to the deglaciation and Heinrich event 1, and the analysis of MIS 1 should also cause higher correlations of paired proxy time series due to the cooling during the Younger Dryas. This can help to test the plausibility of the observed low spatial correlations of Uk'37 LGM proxy records (Fig. 5C).

Conclusions

In this study, we have analysed the correlation structure of temperature proxy records from the LGM that have been collected in close proximity to one another. Spatial correlations were low and only statistically significant for spatial separations <2000 km. For Uk'37, we found no correlation between sites regardless of the distance considered.

To test the consistency between the spatial correlations in the Holocene and LGM, we predicted the expected LGM correlations by accounting for changes in climate variability and time uncertainty. When focusing on planktonic foraminifera Mg/Ca and ice-core stable isotope records, we found consistency between the observed and predicted correlations. In contrast, the observed Uk'37 LGM correlations unexpectedly fell outside the range of the predicted LGM correlations. This suggests that for Uk'37 other effects not accounted for in this study may have caused the inconsistency.

The different behaviour of Uk'37 vs. other proxy types agrees with previous findings (e.g. Lohmann *et al.*, 2013; Liu *et al.*, 2014; Marsicek *et al.*, 2018) and suggests that different proxy types are affected by proxy-specific non-climatic components and uncertainties that may not be fully understood yet. This suggests that analyses using multi-core and multi-proxy datasets (e.g. Reschke *et al.*, 2019a) may be biased by the choice of the proxy type, as some of the underlying assumptions may be oversimplifications of complex climatic and proxy recording processes. Furthermore, the consistency between Holocene and LGM records for planktonic foraminifera Mg/Ca and ice-core stable isotopes after accounting for time uncertainty and changes in climate variability provide some confirmation for the Holocene-based result of low spatial correlations (Reschke *et al.*, 2019a), indicating that current proxy records either record very regional climate signals or have a low signal to noise ratio.

Author contributions—M.R. and T.L. designed the research. M.R. performed the analysis with the aid of I.K. and

wrote the first draft of the manuscript. M.R., I.K. and T.L. contributed to the interpretation and to the preparation of the final manuscript.

Data availability statement

All data that support the findings of this study are related to the dataset of Rehfeld *et al.* (2018), which is available at https://www.nature.com/articles/nature25454#supplementary-information.

Conflict of Interest—The authors declare that they have no conflicts of interest.

Acknowledgements. We thank Torben Kunz and Andrew Dolman for fruitful discussions and comments on the manuscript. The work profited from discussions at the CVAS working group of the Past Global Changes (PAGES) programme. This study was supported by the Initiative and Networking Fund of the Helmholtz Association (grant VG-NH900) as well as the European Research Council (ERC) under the European Union's Horizon 2020 research and innovation programme (grant agreement no. 716092). It further contributes to the German BMBF project PALMOD. I.K. was funded by the Helmholtz Climate Initiative REKLIM (Regional Climate Change), a joint research project of the Helmholtz Association of German Research Centres (HGF). Open access funding enabled and organized by Projekt DEAL.

Appendix A

Deriving the effect of a different signal variance on the correlation

Let us assume that the annually resolved time series X and Y are a superposition of a climate signal, S, and random (white) noises, ε_x and ε_y, as $X = S + \varepsilon_x$ and $Y = S + \varepsilon_y$. Let us further assume that for both time series, all components are uncorrelated (i.e. $cor(S,\varepsilon_x) = cor(S,\varepsilon_y) = cor(\varepsilon_x,\varepsilon_y) = 0$) and the variances σ_s, $\sigma_{\varepsilon x}$ and $\sigma_{\varepsilon y}$ are all equal to 1. Then, the Pearson correlation of X and Y is given by $\rho_{XY} = \frac{cov(X,Y)}{\sqrt{\sigma_X^2}\sqrt{\sigma_Y^2}}$. As signal and noise are uncorrelated, the covariance of X and Y is equal to the variance of the signal component and the characteristics of the noise components are identical, and thus the correlation simplifies to $\rho_{XY} = \frac{\sigma_S^2}{\sigma_S^2 + \sigma_\varepsilon^2}$.

It has been shown that the variance of temperature-sensitive proxy records is higher for the LGM than for the Holocene (Rehfeld *et al.*, 2018). If we assume that the correlation of a time series pair in the Holocene is given by $\rho_{\mathrm{Hol}} = \frac{\sigma_S^2}{\sigma_S^2 + \sigma_\varepsilon^2}$, then we would expect that the variance of the climate signal for the LGM to differ by a factor z, while the noise component would remain the same. Hence, for the LGM the correlation of the time series becomes $\rho_{\mathrm{LGM}}(z) = \frac{z\sigma_S^2}{z\sigma_S^2 + \sigma_\varepsilon^2}$. If we know the Holocene correlation ρ_{Hol} we also know the variance of the noise component which is $\sigma_\varepsilon^2 = \frac{\sigma_S^2}{\rho_{\mathrm{Hol}}} - \sigma_S^2$. Replacing σ_ε^2 simplifies the previous expression to $\rho_{\mathrm{LGM}}(z) = \frac{z}{(z-1) + \rho_{\mathrm{Hol}}^{-1}}$. This is only valid for positive values of ρ_{Hol}, however, due to the underlying assumptions that were made for the time series X and Y.

Supporting information

Additional supporting information may be found in the online version of this article at the publisher's web-site.

Figur S1. Effect of time uncertainty depending on the related timescale of the correlation for a spectral slope of (A) = $\beta_S = 1$ and (B) = $\beta_S = 1.5$. Due to low-pass filtering, climate variability is removed on short timescales, whereas it is still present on long timescales (i.e. all frequencies up to the cut-off frequency f_c). This raises the correlation among time series, assuming the time series contains a superposition of a red noise climate signal and an independent white noise component. The higher the spectral slope β_S of the climate signal (i.e. the 'redder' the climate), the higher is the timescale-dependent correlation after filtering.

Figure S2. Spatial correlation (upper panel) and number of proxy record pairs (lower panel) for the Holocene and LGM. Correlations over distance are summarized in 2000-km-wide bins. The expected spatial correlation for the LGM is based on the reconstructed Holocene spatial correlations without time uncertainty and assumes a higher variance of the signal component ($\mu = 4.4$, $\sigma = 1.15$). The expected correlation of time-uncertain LGM records and its confidence interval (i.e. 90% quantiles) is based on a Monte Carlo procedure with 5000 repetitions applying a time uncertainty of 450 years on time series with a spectral slope of the climate signal of $\beta_S = 1.5$. 90% quantiles of the spatial correlations of uncorrelated Holocene and LGM surrogate data are used as a significance test for the proxy-based spatial correlations. Note that in D and E the correlation estimates between 4000 and 6000 km are based only on Mg/Ca and/or Mg/Ca vs. ice-cores as no ice-core pair at this distance is available.

Figure S3. Orbital trends in seasonal temperatures for (a) the Holocene and (b) LGM, and (c) the latitudinal mean. The temperature differences are based on model simulations of the Holocene (6–0 ka BP; Fischer and Jungclaus, 2011) and the LGM (27–19 ka BP; Zhang *et al.*, 2013). Both time periods exhibit stronger temperature differences in the polar regions than in the tropics.

Table S1. List of records used in this study. This subset is part of the dataset used by Rehfeld *et al.* (2018).

References

Ascough P, Cook G, Dugmore A. 2005. Methodological approaches to determining the marine radiocarbon reservoir effect. *Progress in Physical Geography: Earth and Environment* **29**: 532–547.

Breitenbach SFM, Rehfeld K, Goswami B *et al.* 2012. COnstructing Proxy Records from Age models (COPRA). *Climate of the Past* **8**: 1765–1779.

DeLong KL, Quinn TM, Taylor FW. 2007. Reconstructing twentieth-century sea surface temperature variability in the southwest Pacific: a replication study using multiple coral Sr/Ca records from New Caledonia. *Paleoceanography* **22**: PA4212.

DeLong KL, Quinn TM, Taylor FW *et al.* 2013. Improving coral-base paleoclimate reconstructions by replicating 350 years of coral Sr/Ca variations. *Palaeogeography, Palaeoclimatology, Palaeoecology* **373**: 6–24.

Ditlevsen PD, Svensmark H, Johnsen S. 1996. Contrasting atmospheric and climate dynamics of the last-glacial and Holocene periods. *Nature* **379**: 810–812.

Dolman AM, Laepple T. 2018. Sedproxy: a forward model for sediment-archived climate proxies. *Climate of the Past* **14**: 1851–1868.

Fischer N, Jungclaus JH. 2011. Evolution of the seasonal temperature cycle in a transient Holocene simulation: orbital forcing and sea-ice. *Climate of the Past* **7**: 1139–1148.

Fisher DA, Reeh N, Clausen HB. 1985. Stratigraphic noise in time series derived from ice cores. *Annals of Glaciology* **7**: 76–83.

Gajewski K. 2015. Quantitative reconstruction of Holocene temperatures across the Canadian Arctic and Greenland. *Global and Planetary Change* **128**: 14–23.

Gong C, Hollander DJ. 1999. Evidence for differential degradation of alkenones under contrasting bottom water oxygen conditions:

implication for paleotemperature reconstruction. *Geochimica et Cosmochimica Acta* **63**: 405–411.
Haflidason H, Eiriksson J, van Kreveld SV. 2000. The tephrochronology of Iceland and the North Atlantic region during the Middle and Late Quaternary: a review. *Journal of Quaternary Science* **15**: 3–22.
Harbert RS, Nixon KC. 2018. Quantitative Late Quaternary climate reconstruction from plant macrofossil communities in Western North America. *Open Quaternary* **4**: 1–13.
Hoefs MJL, Versteegh GJM, Rijpstra WIC *et al*. 1998. Postdepositional oxic degradation of alkenones: implications for the measurement of palaeo sea surface temperatures. *Paleoceanography* **13**: 42–49.
Huybers P, Curry W. 2006. Links between annual, Milankovitch and continuum temperature variability. *Nature* **441**: 329–332.
Laepple T, Huybers P. 2013. Reconciling discrepancies between Uk37 and Mg/Ca reconstructions of Holocene marine temperature variability. *Earth and Planetary Science Letters* **375**: 418–429.
Laepple T, Huybers P. 2014. Ocean surface temperature variability: large model–data differences at decadal and longer periods. *Proceedings of the National Academy of Sciences of the United States of America* **111**: 16682–16687.
Laepple T, Münch T, Casado M *et al*. 2018. On the similarity and apparent cycles of isotopic variations in East Antarctic snow pits. *The Cryosphere* **12**: 169–187.
Lea DW. 2003. Elemental and isotopic proxies of past ocean temperatures. In *Treatise on Geochemistry* Vol **6**, Elderfield H, Holland HD, Turekian KK (eds). Elsevier: Amsterdam; 365–390.
Leduc G, Schneider R, Kim J-H *et al*. 2010. Holocene and Eemian sea surface temperature trends as revealed by alkenone and Mg/Ca paleothermometry. *Quaternary Science Reviews* **29**: 989–1004.
Liu Z, Zhu J, Rosenthal Y *et al*. 2014. The Holocene temperature conundrum. *Proceedings of the National Academy of Sciences of the United States of America* **111**: E3501–E3505.
Lohmann G, Pfeiffer M, Laepple T *et al*. 2013. A model-data comparison of the Holocene global sea surface temperature evolution. *Climate of the Past* **9**: 1807–1839.
Luoto TP, Ojala AEK, Arppe L *et al*. 2018. Synchronized proxy-based temperature reconstructions reveal mid- to Late Holocene climate oscillations in High Arctic Svalbard. *Journal of Quaternary Science* **33**: 93–99.
Marcott SA, Shakun JD, Clark PU *et al*. 2013. A reconstruction of regional and global temperature for the past 11,300 years. *Science* **339**: 1198–1201.
Marsicek J, Shuman BN, Bartlein PJ *et al*. 2018. Reconciling divergent trends and millennial variations in Holocene temperatures. *Nature* **554**: 92–96.
Mix AC. 2006. Running hot and cold in the eastern equatorial Pacific. *Quaternary Science Reviews* **25**: 1147–1149.
Mix AC, Bard E, Eglinton G *et al*. 2000. Alkenones and multiproxy strategies in paleoceanographic studies. *Geochemistry, Geophysics, Geosystems* **1**: 2000GC000056.
Morice CP, Kennedy JJ, Rayner NA *et al*. 2012. Quantifying uncertainties in global and regional temperature change using an ensemble of observational estimates: the HadCRUT4 data set. *Journal of Geophysical Research: Atmospheres* **117**: D08101.
Münch T, Kipfstuhl S, Freitag J *et al*. 2016. Regional climate signal vs. local noise: a two-dimensional view of water isotopes in Antarctic firn at Kohnen Station, Dronning Maud Land. *Climate of the Past* **12**: 1565–1581.
Münch T, Kipfstuhl S, Freitag J *et al*. 2017. Constraints on post-depositional isotope modifications in East Antarctic firn from analysing temporal changes of isotope profiles. *The Cryosphere* **11**: 2175–2188.
Ohkouchi N, Eglinton TI, Keigwin LD *et al*. 2002. Spatial and temporal offsets between proxy records in a sediment drift. *Science* **298**: 1224–1227.
Regenberg M, Nürnberg D, Steph S *et al*. 2006. Assessing the effect of dissolution on planktonic foraminiferal Mg/Ca ratios: evidence from Caribbean core tops. *Geochemistry, Geophysics, Geosystems* **7**: Q07P15.
Rehfeld K, Münch T, Ho SL *et al*. 2018. Global patterns of declining temperature variability from the Last Glacial Maximum to the Holocene. *Nature* **554**: 356–359.
Reschke M, Kunz T, Laepple T. 2019b. Comparing methods for analysing time scale dependent correlations in irregularly sampled time series data. *Computers and Geosciences* **123**: 65–72.
Reschke M, Rehfeld K, Laepple T. 2019a. Empirical estimate of the signal content of Holocene temperature proxy records. *Climate of the Past* **15**: 521–537.
Shakun JD, Clark PU, He F *et al*. 2012. Global warming preceded by increasing carbon dioxide concentrations during the last deglaciation. *Nature* **484**: 49–54.
Stephans CL, Quinn TM, Taylor FW. 2004. Assessing the reproducibility of coral-based climate records. *Geophysical Research Letters* **31**: L18210.
Stuiver M, Pearson GW, Braziunas T. 1986. Radiocarbon age calibration of marine samples back to 9000 cal yr BP. *Radiocarbon* **28**: 980–1021.
Wei W, Lohmann G. 2012. Simulated Atlantic Multidecadal Oscillation during the Holocene. *Journal of Climate* **25**: 6989–7002.
Zhang X, Lohmann G, Knorr G *et al*. 2013. Different ocean states and transient characteristics in Last Glacial Maximum simulations and implications for deglaciation. *Climate of the Past* **9**: 2319–2333.

